Applied Water Science (2020) 10:169
https://doi.org/10.1007/s13201-020-01255-7

ORIGINAL ARTICLE

Effect of 90° elbows on pump inlet flow conditions

Ronaldo Novaes Ferreira[1] · Leonardo Machado da Rosa[2] · Johannes Gérson Janzen[1,3]

Received: 24 May 2019 / Accepted: 11 June 2020 / Published online: 24 June 2020

Abstract
The use of 90° elbows upstream of a pump inlet can distort the approach flow resulting in spatial and temporal velocity variations and swirling flow that negatively affect pump performance and increase maintenance requirements. In order to attend these flow conditions, pumps have to be installed according to generally accepted standards such as ANSI/HI 9.8. (American national standard for rotodynamic pumps for pump intake design, Hydraulic Institute, Parsippany, 2012). However, in these standards, there is little information about the minimum distance between single and double 90° elbows and a pump. Therefore, this paper presents results for the pipe flow downstream of 90° elbows and its attendance to the standards at the inlet of pumps using Computational Fluid Dynamics (CFD). Prior to its application, the CFD model was validated by comparing the computed velocity profiles with experimental results downstream of a 90° elbow. It is found that it is necessary 3 to 16 pipe diameters from the elbow in order to reduce the swirling flow. The velocity distribution at a cross section was never uniform up to 50 pipe diameters downstream of the elbows. The temporal velocity fluctuation was always low. It is concluded that the specifications of downstream pipe lengths in the current inlet pipe flow standards are not sufficient to achieve the desired flow at the pump inlet.

Keywords CFD · Swirl · Velocity distribution

Introduction

The flow in 90° curved pipes has for long captured the attention of fluid physics community both from a fundamental and an applied view (Ono et al. 2011). Curved pipes can be found as part of nearly all industrial and engineering systems due to space limitations and to the need for altering the direction of the fluid motion (Mittag and Gabi 2015). In engineering application of pumping systems, turning flow just upstream of a pump inlet can distort the approach flow resulting in spatial and temporal velocity variations and swirling flow that negatively affect pump performance and increase maintenance requirements ((Mahaffey and van Vuuren 2014). A non-uniform velocity profile at the pump inlet can result in pump's lower efficiency (less than its Best Efficiency Point-BEP), oscillating power requirements, and pump's damage (Khan and Islam 2012). Furthermore, spatial and temporal velocity fluctuations at the pump inlet can cause pressure fluctuations on the pump impeller and, consequently, a loading imbalance on the pump shaft, possibly causing vibration or pre-mature bearing wear (Khan and Islam 2012). Finally, swirling flow results in flow hitting the impeller blade at an angle of attack other than what it was designed for, producing localized flow separation on the impeller and low-pressure regions, hence causing cavitation in localized areas (Khan and Islam 2012).

Given these potential impacts on pump performance and maintenance requirements, the following pump inlet flow conditions are typically prescribed in the literature (e.g., ANSI/HI 9.8 2012): (i) The average swirl angle should be less than 5° (swirl angle $\theta = \tan^{-1}(V_\theta/U)$, where V_θ is the tangential velocity and U is the axial velocity); (ii) time-averaged velocities at the pump suction shall be within 10% of the cross-sectional average velocity; (iii) The temporal velocity fluctuations should be less than 10% of the cross-sectional averaged velocity at that location.

✉ Johannes Gérson Janzen
johannesjanzen@gmail.com

[1] Faculty of Engineering, Architecture and Urbanism and Geography, Federal University of Mato Grosso do Sul, Campo Grande, Brazil

[2] Regional University of Blumenau, Blumenau, Brazil

[3] Universidade Federal de Mato Grosso do Sul, Av. Costa e Silva, s/nº, Bairro Universitário, Campo Grande, Mato Grosso do Sul 79070-900, Brazil

In order to attend these prescribed flow conditions the norms for pump intake design usually recommend that there shall be no short radius elbows ($Rc/D < 1.5$) closer than 5 suction pipe diameters from the pump, and that long radius elbows ($Rc/D > 1.5$) and reducers do not disturb the flow (e.g., ANSI/HI 9.8 2012). However, very little information is available in the literature, discussing which distance from the pump is sufficient to attend the three flow conditions described above for short and long radius and reducing elbows are capable to attend the three pump inlet flow conditions described above (Allen et al. 2015).

Therefore, the goal of this paper is to investigate to what extent the flow downstream from elbows attend the above-described pump inlet flow conditions. In order to achieve this goal, we performed a series of computational modeling for short and long radius elbows using Computational Fluid Dynamics (CFD). Furthermore, we used literature data to validate the used models. Results indicate that the standards mentioned above need to have the installation specifications improved.

Materials and methods

A schematic diagram of the setup is shown in Fig. 1. The setup consisted of a smooth pipe with an inner diameter (D) of 0.25 m. Those values were chosen based on real pumping stations. The fluid considered was water at the temperature of 298 K (24.85 °C), which corresponds to a density (ρ) of 997 kg/m^3 and a dynamic viscosity (μ) of 8.899.10^{-4} kg/(ms). The first pipe configuration had an initial length of 40D of straight pipe before entering a 90° elbow (to achieve a developed flow), followed by another straight section of 50D. In this configuration, two elbow curvatures (Rc/D), 1 (Fig. 1a) and 1.296 (Fig. 1b), were investigated. The Reynolds number, Rey = UD/ν (where ν is the kinematic viscosity), ranged from $5x10^3$ to $5x10^5$.

The second configuration had an initial length of 40D of straight pipe before entering a 90° elbow (to achieve a developed flow), followed by another straight section of 3.5D, followed by a second 90° elbow, and finally a straight section of 50D long. In the first case, both elbows had $Rc/D = 1.296$ (Fig. 1c); in the second case, we used a ratio of $Rc/D = 1.492$ for the first elbow and a ratio of $Rc/D = 3.348$ for the second elbow (Fig. 1d). The Reynolds number, Rey, ranged from $5x10^3$ to $5x10^5$.

The American National Standard for Pump Intake Design guidelines (ANSI/HI 9.8, 2012) were followed to evaluate the Reynolds number and setup effect on the flow conditions downstream a 90° elbow. Those guidelines present design and operational recommendations on model pump intakes and the best flow conditions before a pump's inlet, in order to guarantee best pump performance. Although pumps were not simulated in the present study, the pipe design must provide adequate conditions at the pump inlet, thus these guidelines were applied. The following criteria were applied to

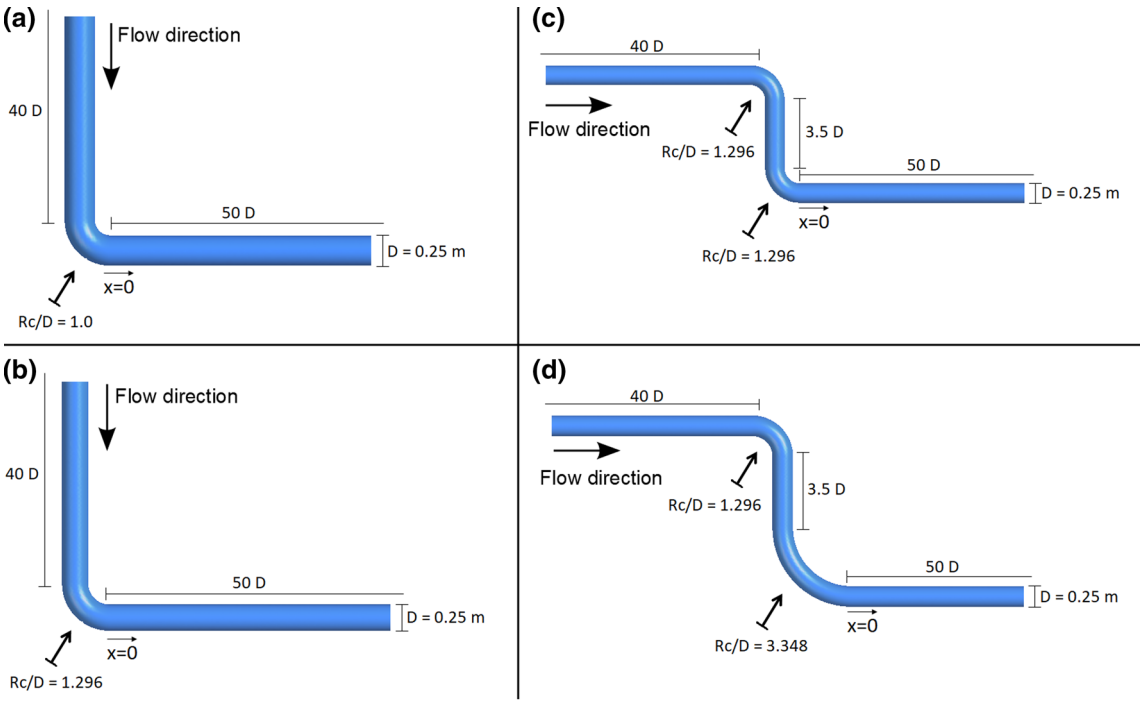

Fig. 1 Side view of the generated geometries. **a** Setup 1; **b** Setup 2; **c** Setup 3; **d** Setup 4

the studied cases: (i) Swirl angles must be less than 5°; (ii) Time-averaged velocities at the pump suction in a piping system shall be within 10% of the cross-sectional area average velocity; (iii) The temporal velocity fluctuations should be less than 10 percent of the cross-sectional averaged velocity at that location. The time-averaged axial velocity U was determined as follows: $U = \int_0^T u(t)\mathrm{d}t$ (where $u(t)$ is the instantaneous velocity at a point and T is the averaging time). The temporal velocity fluctuation was $u'(t) = u(t) - U$.

The flow field was obtained through three-dimensional transient simulations by solving the Reynolds Averaged Navier–Stokes (RANS) equations. The RNG k–ε turbulence model was used, along with wall functions, to account for the turbulent characteristics of the flow and is presented in detail by Koutsourakis et al. (2012). Kim et al. (2014) showed that the RNG k-ε turbulence model gives good results for primary streamwise velocity and secondary swirling velocity profiles induced by 90° elbow in turbulent pipe flow, when compared to other turbulence models. The commercial Computational Fluid Dynamics (CFD) code ANSYS CFX version 14.5.7 was used to solve the equations. The power-law discretization scheme was used for the momentum, turbulent kinetic energy and the turbulent energy dissipation rate. The solution was iterated until the convergence was achieved (i.e., the residue for each equation fell below 10^{-6}) or the modeling time of 70 s was achieved. The time step was of 0.05 s. Preliminary simulations show the full development of the flow after 70 s.

Boundary conditions were defined at the borders of the computational domain. At the inlet, a uniform flow velocity U was imposed with turbulent kinetic energy $k = 1.5(I.U)^2$ (where I is the turbulence intensity equal to $0.16\mathrm{Rey}^{-0.125}$), and specific dissipation rate $\varepsilon = (C_\mu k^{3/2})/0.3D$ ($C_\mu = 0.0845$). At the outlet, an average static reference pressure of 0 Pa was specified. A no-slip boundary condition was applied at the walls.

The numerical model was first validated using the experimental measurements presented by Kim et al. (2014). The authors used a pipe with an internal diameter of 50.8 mm. The elbow had a radius of curvature of 152.4 mm (3D), and the lengths of the upstream and downstream sections were 3.35 m ($L/D = 66$) and 9.1 m ($L/D = 180$), respectively. A fully structured 3D mesh was used containing hexahedral elements. The number of elements was defined after a grid uncertainty evaluation, following the procedures presented by Celik et al. (2008). Three progressively finer grids were employed: a coarse grid with 575,564 elements; a medium grid with 1,306,115 elements; and a fine grid with 2,876,357 elements. The coarse grid has as uncertainty of 1.57% and the medium grid of 1.74%. Due to the small differences in the results and the higher number of elements for the medium and fine grids, the coarse grid was chosen for further calculations.

Experimental results from Kim et al. (2014) were used to validate the models used. The simulated results show good agreement with the experimental ones for both symmetry and cross-mean axial velocity profile lines (Fig. 2). The discrepancies between numerical and experimental data, especially for the 3.5D case, occur as a result of adverse pressure gradient near the inner wall of the elbow. Nonetheless, the error observed between experimental and numerical values is lesser than 7%.

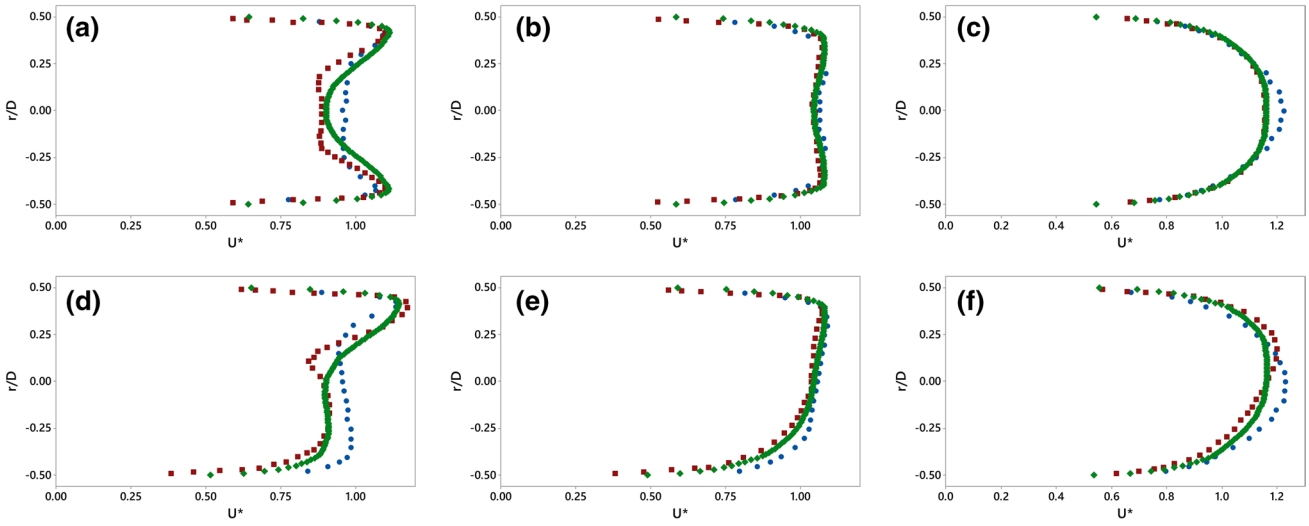

Fig. 2 Numerical and experimental comparison of non-dimensional velocity, $U^* = U/U_m$ (U_m is the average velocity). Along cross or 0° lines for **a** 3.5D, **b** 10D, and **c** 50D. Along symmetric or 90° lines for **d** 3.5D, **e** 10D, and **f** 50D. ● Experimental data (Kim et al., 2014); ■ RNG k-e (Kim et al., 2014); ♦ RNG k-e (present work)

Results and discussion

Figures 3b and d show the cross-sectional mean velocity distributions at different positions for Setups 2 and 3, respectively. Upstream of the first elbow, the velocity profile is fully developed. At the elbow outlet, as observed by previous investigators (e.g., Sudo et al. 1992), there is a shift of the peak velocity toward the outer wall of the elbow due to the outward secondary flow, and a region having very low velocity is formed between the inner wall and the center of the pipe. The water with low velocity near the inner wall shifts toward the central region of the pipe, increasing gradually the velocity of the water near the inner wall. The region of low velocity moves farther toward the outer wall, and the secondary flow weakens gradually, its cores shifting to the central part of the pipe. Further downstream, the secondary flow breaks down and the longitudinal velocity shows a smooth distribution without unevenness. However, a further longitudinal distance is required for the flow to exhibit a symmetric velocity distribution, as shown in the upstream tangent.

The spatial non-uniformity of the velocity at the pump inlet can cause pressure fluctuations on the pump impeller and, consequently, a loading imbalance on the pump shaft, possibly causing vibration or pre-mature bearing wear (Khan and Islam 2012). The overall acceptability of the velocity profile at the pump inlet has been based on the ratio of the minimum and maximum velocities, U_{min} and U_{max}, respectively, to the average velocity, U_m ($U^*_{max} = U_{max}/U_m$ and $U^*_{min} = U_{min}/U_m$). The velocity profile is acceptable for the pump inlet once a cross section is able to produce velocities that are within 10% of the average velocity. Figure 4 shows U^*_{max} and U^*_{min} in function of x/D. Initially the curves distanced themselves from the dashed line (10% of the average velocity), then for a

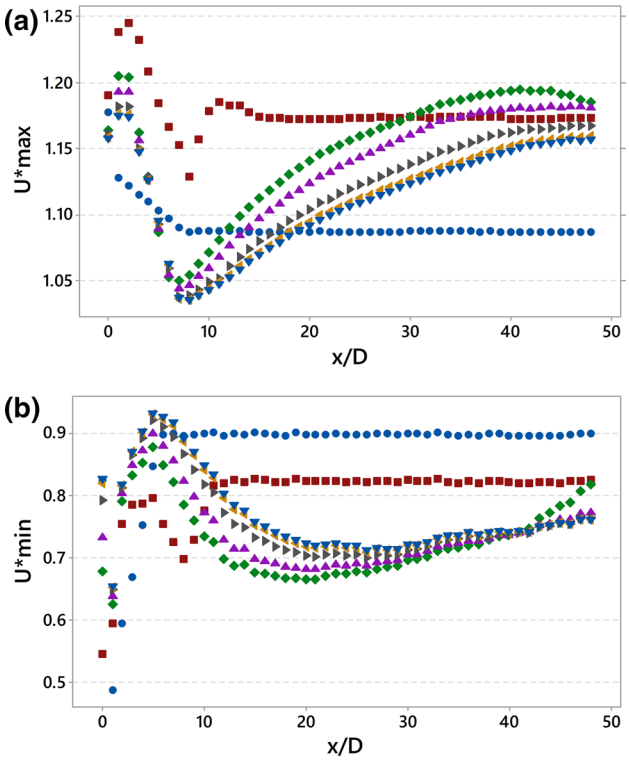

Fig. 4 **a** Maximum and **b** minimum time-averaged velocities along the pipe after a long elbow (Setup 2). The velocities should be within 10% of the cross-sectional area average velocity. ● Rey = 5,000; ■ Rey = 10,000; ♦ Rey = 50,000; ▲ Rey = 100,000; ► Rey = 250,000; ◄ Rey = 425,000; ▼ Rey = 500,000

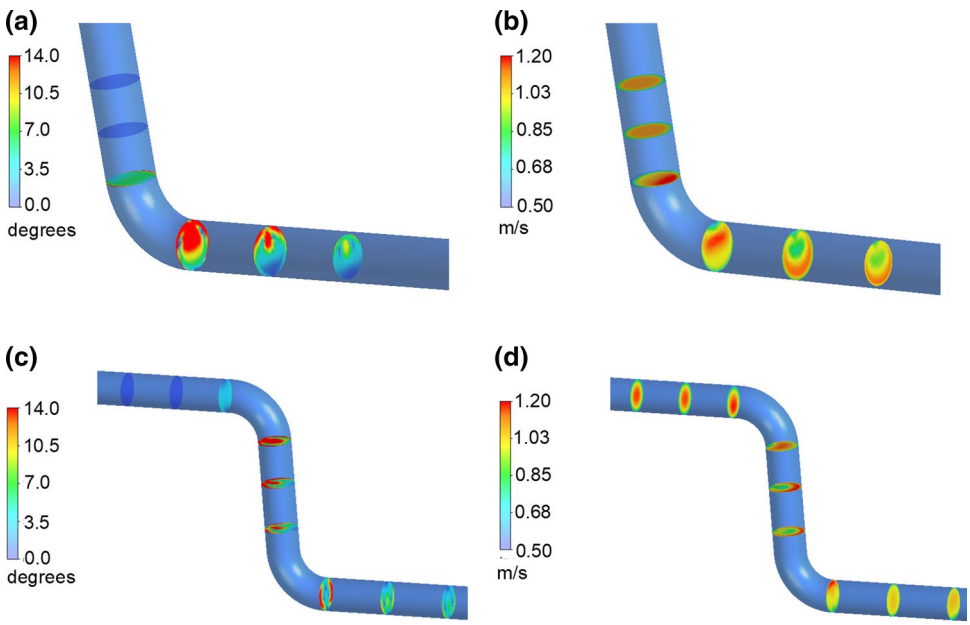

Fig. 3 Setup 2: **a** Contour map of swirl angle S, and **b** streamwise velocity U^*; Setup 3: **c** Contour map of swirl angle S, and **d** streamwise velocity U^*

short-space, the curves remain inside the 10% region, and, finally, they tend to the values of the fully developed flow.

Figure 5 presents U^*_{max} and U^*_{min} in function of Reynolds number (Rey) for different curvature radius (Rc/D_{in}) and distances from the elbow. Although in general U^*_{max} decreases with increasing Reynolds, and U^*_{min} increases with increasing Reynolds, the values of U^*_{max} and U^*_{min} are never concomitantly within 10% of the average velocity. Enayet et al. (1982), Sudo et al. (1992), Ono et al. (2011), Hellström et al. (2013), and Kim et al. (2014) also observed velocity variation bigger than 10% of the cross-sectional average velocity Reynolds between 25,000 and 115,000, and for distances up to 50D downstream of the curve. It is worth to mention that we are ignoring the boundary layer effects.

In order to explain these velocities bigger than 10% of the cross-sectional average velocity, we considered the empirical power-law equation as a good approximation for the velocity profile for fully developed turbulent flow through a smooth pipe (e.g., Fox et al. 2008), as follows

$$\frac{u}{U_{max}} = \left(1 - \frac{r}{R}\right)^{\frac{1}{n}} \quad (1)$$

where the exponent, n, varies with Rey according to equation

$$n = -1.7 + 1.8\log(\text{Rey}) \quad (2)$$

U^*_{max} may be calculated for the power-law profiles of Eq. (1) assuming the profiles from the wall to the centerline, resulting in

$$U^*_{max} = \frac{(n+1)(2n+1)}{2n^2} \quad (3)$$

U^*_{max} decreases with increasing Reynolds number (i.e., increasing exponent n) (Fig. 6). For $n < 14$ (i.e., $\text{Rey} < 1.28x10^8$), U^*_{max} is bigger than 1.1. Therefore, even for fully developed turbulent flow, for a large range of Reynolds number the velocity variation is bigger than 10% of the cross-sectional average velocity.

ANSI/HI 9.8 (2012) specifies that time velocity fluctuations at a point shall produce a standard deviation from the time-averaged signal of less than 10%. The observed temporal velocity variation is smaller than 10% for any setup and Reynolds (not shown in this text). Hence, all cases attend the criterion specified by the norm.

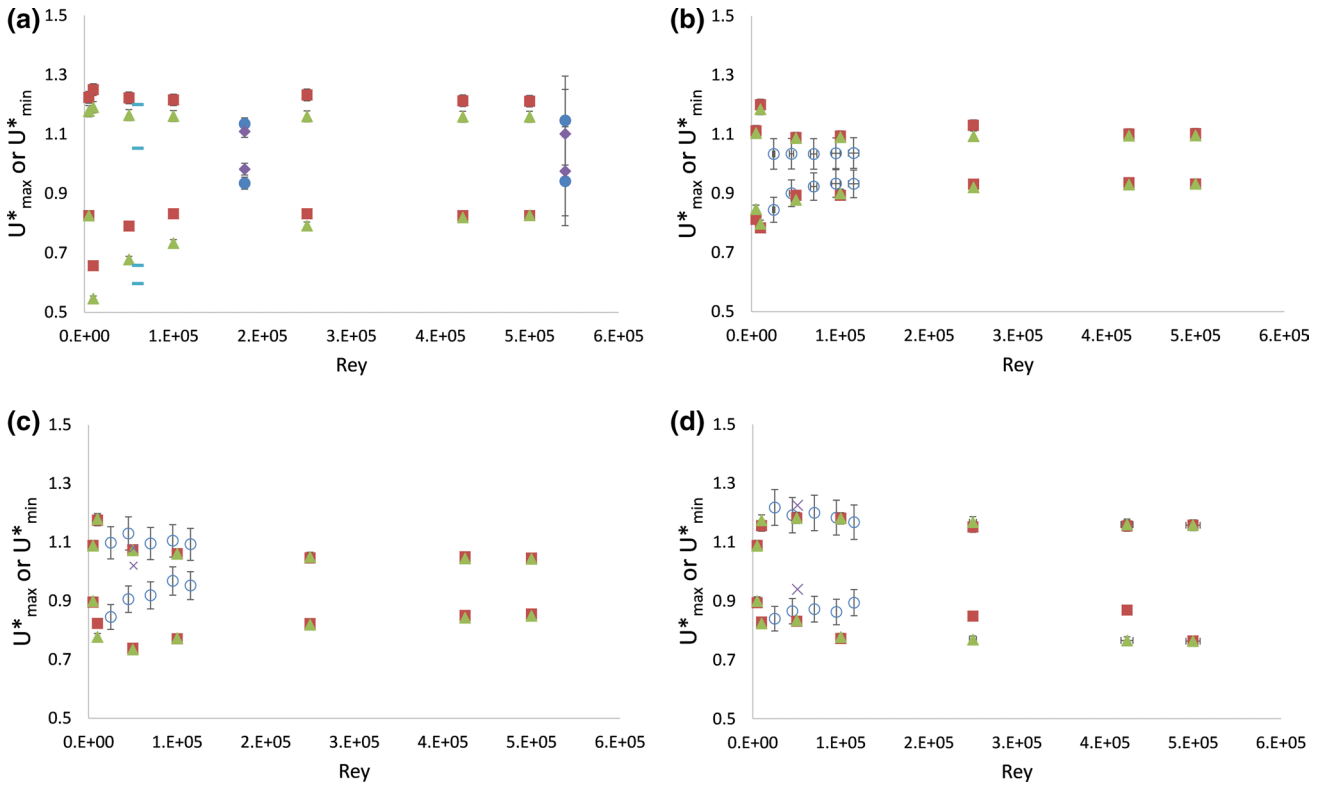

Fig. 5 Maximum and minimum time-averaged velocities along the pipe after a 90-degree elbow. The velocities should be within 10% of the cross-sectional area average velocity. **a** $x/D = 0$; **b** $x/D = 5$; **c** $x/D = 10$; **d** $x/D = 50$. ○ Rc/D = 1.0 (Hellström et al., 2013); ● Rc/D = 1.0 (Ono et al., 2011); ■ Rc/D = 1.0 (present work); ▲ Rc/D = 1.296 (present work); ◆ Rc/D = 1.5 (Ono et al., 2011); ▬ Rc/D = 2.0 (Sudo et al., 1992); x Rc/D = 3.0 (Kim et al., 2014)

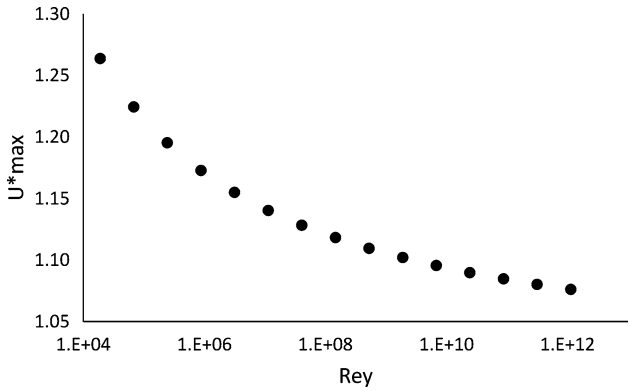

Fig. 6 U^*_{max} in function of *Rey*, considering Eqs. (1) to (3)

The axial development of the maximum swirl angle S_{max}, determined by the ratio of the circumferential and axial velocity, is given in Figs. 4a and c, respectively, for Setups 2 and 3. Swirl angles entering the pump must be less than 5°. On all cases, after increasing right after the elbow, *S* decreases along the rest of the pipe, with a dependency on the Reynolds number and the kind of setup (Fig. 7).

The decay of swirl is caused by transport of angular momentum to the pipe wall (Steenbergen and Voskamp 1998). Using the angular momentum equation, and assuming that the change in the flux of angular momentum is balanced by the wall shear stress, Steenbergen and Voskamp (1998) showed that the decrease swirl intensity with *x/D* in turbulent pipe flow can be approximated by an exponential decay function. Since the swirl angle may serve as a reliable estimate of the swirl number, the swirl angle decay can be expressed as follows

$$S_{\max} = ae^{-b\frac{x}{D}} \tag{4}$$

where *a* and *b* are constants. The rate of decay of the swirl is expressed by the coefficient *b*, varying with the Reynolds number. For turbulent flow in straight pipes with a smooth wall, *b* is directly proportional to the friction factor (Steenbergen and Voskamp 1998). The decay rate decreases as the Reynolds number increases (Fig. 8b), which agrees with the results of Mattingly and Yeh (1991). For Rey $\leq 10^4$, there was a strong influence of Reynolds upon maximum swirl angle; for Rey $> 10^4$, *S* had a weak dependence on Reynolds number, agreeing with the more recent results of Kim et al. (2014) and (Dutta et al. 2016). For the one-elbow setups, *S* had a low dependence on curvature radius, agreeing with the results of Kim et al. (2014) for $Rc/D \leq 3.49$. For the two-elbow setups, the different *Rc/D* of the second elbow had an influence upon the maximum swirl angle.

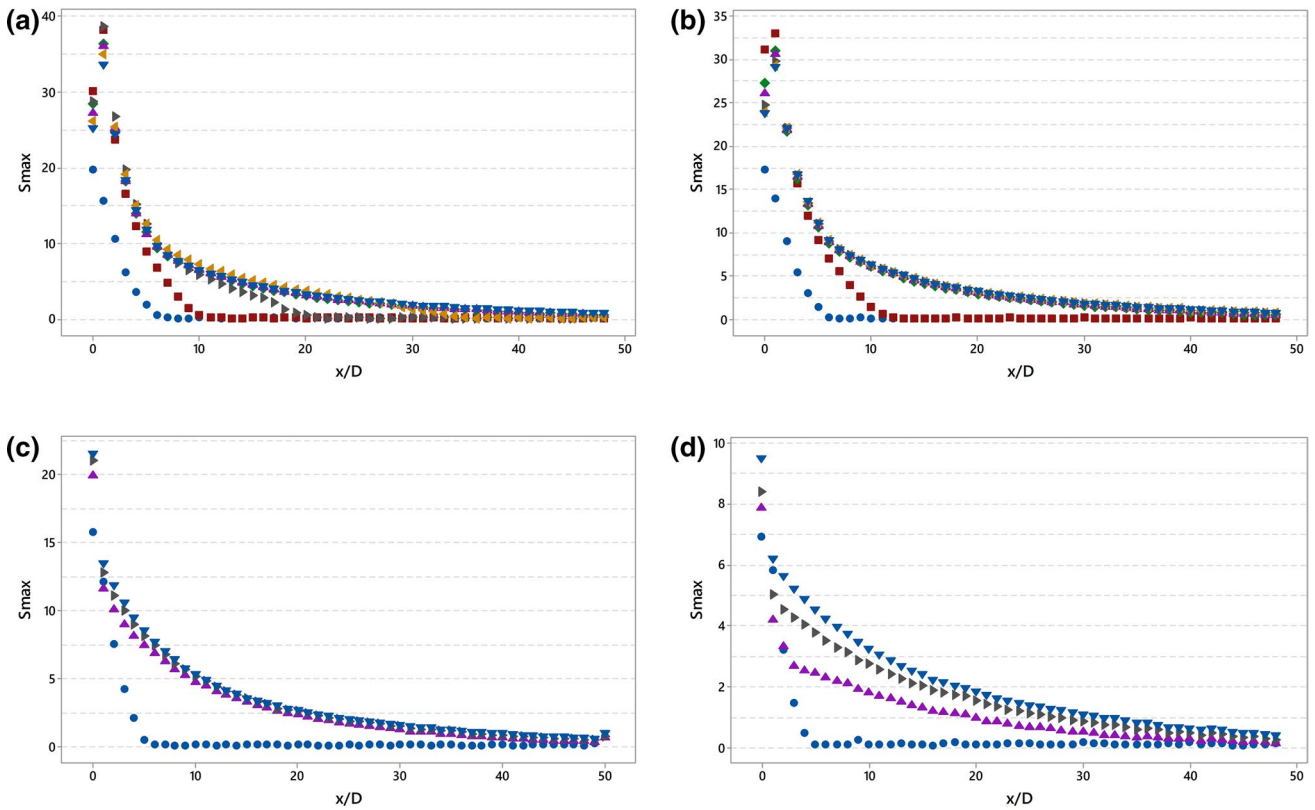

Fig. 7 Maximum swirl angle distribution along the pipe. 5 degrees is the desirable value. **a** Setup 1; **b** Setup 2; **c** Setup 3; **d** Setup 4. ● Rey = 5000; ■ Rey = 10,000; ♦ Rey = 50,000; ▲ Rey = 100,000; ► Rey = 250,000; ◄ Rey = 425,000; ▼ Rey = 500,000

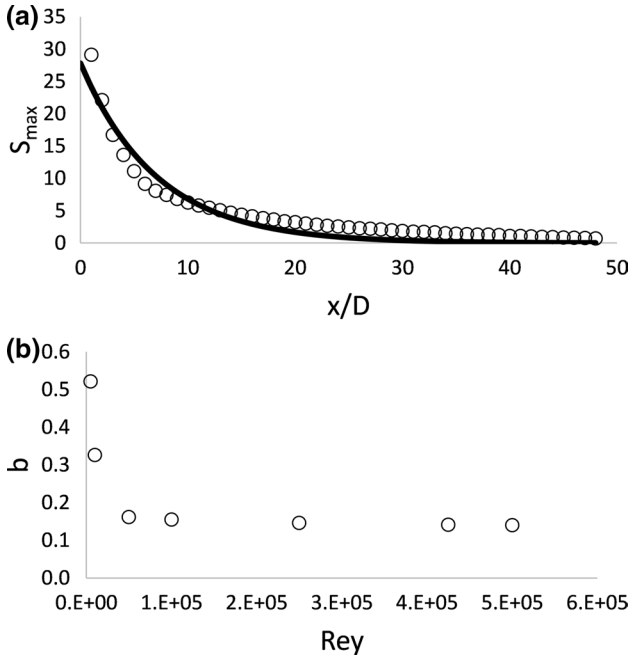

Fig. 8 **a** Decay of maximum swirl angle along straight pipe after elbow for Setup 2 and *Rey* = 500,000, (◌) our results, (line) Eq. 4. **b** Decay rate *b* (see Eq. 4) in function of Reynolds number for Setup 2

The distance required by the flow to have the maximum swirl angle reduced to $S = 5°$, *Ls*, is plotted in Fig. 9 in relation to the Reynolds number for the different setups. In general, the maximum swirl angle increased with the increase in Reynolds number. Setups 1 and 2 had similar tendencies, since *Ls* increased from 4*D*, at Reynolds number equal to 5000, to approximately 14*D*, for Reynolds number equal (and greater) to 5.10^4. Hence, for the one-elbow setups, *Rc* had a weak influence upon *Ls*.

As already mentioned, Steenbergen and Voskamp (1998) showed that for turbulent swirling flows in straight pipes with smooth wall the dependence of the swirl decay rate on the Reynolds number is similar to that of the friction factor. Since the friction factor decreases with increasing Reynolds, the swirl angle also decreases. This means that as the Reynolds number increases, the rate of decrease in the friction factor diminishes. In a similar way, the swirl angle decay rate should also diminish with increasing Reynolds numbers. Consequently, the increase in *Ls* with Rey for a given setup should become smaller for increasing Reynolds numbers, as observed for $\text{Rey} > 5.10^4$ (Fig. 9).

Note that the effect of wall roughness was not investigated. The discussion above was for smooth pipes. However, if we consider that the swirl decay rate is proportional to the friction factor, and that the friction factor is almost independent of the Reynolds number (valid only for a region of the Moody diagram), then *Ls* would have a similar behavior then that found in Fig. 9. However, since the influence of wall roughness was not modeled, this result should be taken cautiously, and included as a future work.

For the two-elbow setups, the swirl is much more complicated, being a composite of two types of swirl, depending on the pipe length between the two elbows (Mattingly and Yeh 1991). For a long pipe length between the two elbows, the swirl should approach that of a single elbow case. The comparison of *Ls* from Setup 2 with Setup 3 show that, for Setup 3, the swirl produced by the first elbow still has an influence upon the swirl produced by the second elbow, tending to 11*D*. Finally, Setup 4, with the highest *Rc*, promoted the lowest swirl angle values of all setups and Reynolds numbers, reaching an angle of 5° within 5*D* for all Reynolds numbers.

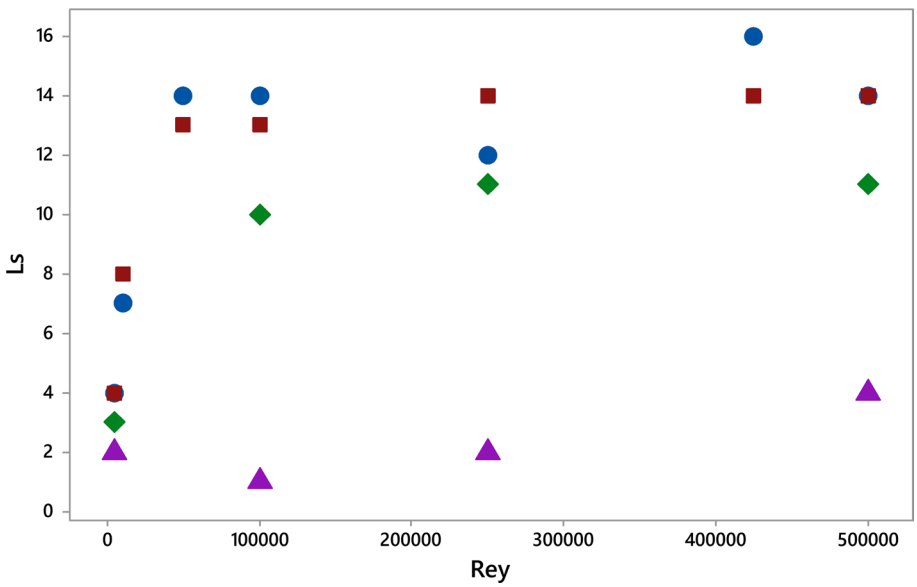

Fig. 9 Distances (*Ls*) in which each Setup reached 5° for the swirl angle in function of the Reynolds number. ● Setup 1; ■ Setup 2; ◆ Setup 3; ▲ Setup 4

These numerical results can be used to evaluate the current specifications of ANSI/HI 9.8 (2012). Firstly, it can be observed that all elbows (or Setups) fall outside of the acceptance criteria, mainly because the velocity variation along the cross section is more than 10% of the average velocity along the cross section, i.e., this criterion must either be reviewed or better specified by the norm. This concern agrees with the conclusions presented by Verhaart et al. (2015), who stated that the criteria of the norm are not sufficiently clearly defined. Secondly, to reduce the swirl angle to less than 5° for short radius elbows, a length from 3*D* to 16*D* would be required. The ANSI/HI 9.8 (2012) specification of 5*D* for short radius elbows is not sufficient. Furthermore, long radius elbows cannot be considered as not flow-disturbing fittings as assumed by the norm, since they fall outside of two acceptance criteria, namely that the average swirl angle should be less than 5°, and that the time-averaged velocities at the pump suction shall be within 10% of the cross-sectional area average velocity.

Conclusion

A three-dimensional CFD model of different setups of a 90° elbow is presented in this paper. The CFD model predicted at several sections the time-averaged velocities, the time velocity fluctuations, and the swirl angle. Our results indicate that the maximum swirl angle was less than 5° for 3*D* to 16*D* from the elbow. The velocity deviation of point temporal velocity from the time-averaged mean were less than 10%. Finally, the velocity variation along the cross section was greater than 10% of the cross-sectional average velocity for all modeled setups and all data found in the literature. Therefore, this criterion must either be reviewed or better specified by the norm.

Funding Johannes G. Janzen received funding from CAPES (Coordination for the Improvement of Higher Education Personnel - Programa de Professor Visitante no Exterior - 88881.170363/2018-01). Johannes also thanks the Institutional Program of Internationalization sponsored by CAPES (Capes-Print).

Compliance with ethical standards

Conflict of interest The authors declare that they have no conflict of interest.

References

Allen ME, Werth DE, Allaben CC (2015). An evaluation of reducing elbow characteristics versus velocity distribution at the pump inlet. In: Proceedings of the world environmental and water resources Congress 2015: Floods, Droughts, and Ecosystems

ANSI/HI 9.8. (2012) American national standard for rotodynamic pumps for pump intake design. Hydraulic Institute, Parsippany

Celik IB, Ghia U, Roache PJ, Freitas CJ, Coleman H, Raad PE (2008) Procedure for estimation and reporting of uncertainty due to discretization in CFD applications. ASME J Fluids Eng 130(7):078001-078001-4. https://doi.org/10.1115/1.2960953

Dutta P, Saha SK, Nandi N, Pal N (2016) Numerical study on flow separation in 90° pipe bend under high Reynolds number by k-ε modelling. Eng Sci Technol Int J 19(2):904–910. https://doi.org/10.1016/j.jestch.2015.12.005

Enayet M, Gibson MM, Taylor AMKP, Yianneskis M (1982) Laser-Doppler measurements of laminar and turbulent flow in a pipe bend. Int J Heat Fluid Flow 3(4):213–219. https://doi.org/10.1016/0142-727X(82)90024-8

Fox RW, McDonald AT, Pritchard PJ (2008) Introduction to fluid mechanics. Wiley, Hoboken

Hellström L, Zlatinov M, Cao G, Smits A (2013) Turbulent pipe flow downstream of a 90° bend. J Fluid Mech 735:R7-1–R7-12. https://doi.org/10.1017/jfm.2013.534

Khan LA, Islam A (2012) CFD Modeling to Evaluate design of an intake of a raw water pump station at a water treatment plant. In: Proceedings of the world environmental and water resources congress 2012: Crossing Boundaries

Kim J, Yadav M, Kim S (2014) Characteristics of secondary flow induced by 90-degree elbow in turbulent pipe flow. Eng Appl Comput Fluid Mech 8(2):229–239. https://doi.org/10.1080/19942060.2014.11015509

Koutsourakis N, Bartzis JG, Markatos NC (2012) Evaluation of Reynolds stress, k-ε and RNG k-ε turbulence models in street canyon flows using various experimental datasets. Environ Fluid Mech 12(4):379–403. https://doi.org/10.1007/s10652-012-9240-9

Mahaffey RM, Van Vuuren SJ (2014) Review of pump suction reducer selection: eccentric or concentric reducers. J S Afr Inst Civ Eng [online] 56(3):65–76

Mattingly GE, Yeh TT (1991) Effects of pipe elbows and tube bundles on selected types of flowmeters. Flow Meas Instrum 2(1):4–13. https://doi.org/10.1016/0955-5986(91)90050-2

Mittag S, Gabi MJ (2015) Experimental and numerical investigation of centrifugal pumps with asymmetric inflow conditions. Therm. Sci. 24(6):516–525. https://doi.org/10.1007/s11630-015-0817-8

Ono A, Kimura N, Kamide H, Tobita A (2011) Influence of elbow curvature on flow structure at elbow outlet under high Reynolds number condition. Nucl Eng Des 241:4409–4419. https://doi.org/10.1016/j.nucengdes.2010.09.026

Steenbergen W, Voskamp J (1998) The rate of decay of swirl in turbulent pipe flow. Flow Meas Instrum 9(2):67–78. https://doi.org/10.1016/S0955-5986(98)00016-8

Sudo K, Sumida M, Yamane R (1992) Secondary motion of fully developed oscillatory flow in a curved pipe. J Fluid Mech 237:189–208. https://doi.org/10.1017/S0022112092003380

Verhaart FIH, Fockert A, Zwanenburg SAA (2015) Velocity profiles in the bell mouth throat of vertically submersible pumps. J Appl Water Eng Res 4(2):102–111. https://doi.org/10.1080/23249676.2015.1090350